CONTINUOUS LASER SCAN STRATEGY FOR FASTER BUILD SPEEDS IN LASER POWDER BED FUSION SYSTEM

H. Yeung[1], B. Lane[1], J. Fox[1], F. Kim[1], J. Heigel[1], J. Neira[2]

[1]Engineering Laboratory, [2]Physical Measurement Laboratory,

National Institute of Standards and Technology, Gaithersburg, MD 20899

Abstract

Research has shown significant influence of laser scan strategy on various part qualities in the laser powder bed fusion additive manufacturing process. The National Institute of Standards and Technology developed the Additive Manufacturing Metrology Testbed, which provides open architecture for flexible control and monitoring during a laser powder bed fusion additive manufacturing process. This allows extended control of scan strategies, including control of laser power and speed within each scan line. A 'continuous' scan strategy can reduce build times and improve throughput by negating the need to turn the laser off between scan tracks (e.g., sky-writing). Also, less frequent laser power interruption can potentially improve the melt-pool continuity. Multiple experiments are performed utilizing the continuous and traditional scan strategies, and comparisons are made between build time and measured melt-pool qualities.

Introduction

Laser powder bed fusion (LPBF) is an additive manufacturing (AM) process in which a focused, high power laser selectively melts geometric patterns into layers of metal powder, ultimately building a near fully dense freeform part. The LPBF fabricated part quality is determined by many process parameters [1], such as the laser scan strategies (position, power, and velocity) and their respective synchronization, in conjunction with powder layer parameters (material, relative density, layer height, etc.). Varying the relative combination of these parameters can introduce known defects that plague LPBF parts. Pores, for example, have been attributed to various phenomena related to the power-velocity attributes or scan strategies (e.g., keyholing and collapse at high laser energy densities [2], or insufficient re-melting of adjacent scan vectors due to wide hatch spacing [3,4]). For example, Khairallah et al. noted that turning the laser off at the end of a scan vector can potentially cause pores to be trapped under the rapidly solidified melt pool, and recommended laser power decreased at these locations [5]. More adequately controlled velocity or power profiles along each scan vector can reduce probability of pore formation, or provide a parametric space for other property optimization. Apart from solidification physics at the end of a single vector, the general size, shape, and timing of a laser scanning raster pattern are known to affect the melt pool thermal history of the part, thus the resulting local and global residual stress and microstructure [6–8].

Though LPBF technologies are rapidly improving and maturing, there is still wide potential for research in melt pool, scan track, and layer formation process physics. To fully define scan strategies, a system needs to control both how to fill up the build areas with scan vectors (hatching), and position, power, and velocity of individual scan vectors. The National Institute of Standards and Technology (NIST) designed and built an open architecture Additive Manufacturing Metrology Testbed (AMMT). The control software developed for AMMT utilizes the full access of system parameters to enable quick deployment of different scan strategies. This work compares three scan strategies implemented on AMMT: continuous linear, continuous concentric, and constant build speed (sky-writing).

Certain commercial entities, equipment, or materials may be identified in this document in order to describe an experimental procedure or concept adequately. Such identification is not intended to imply recommendation or endorsement by the National Institute of Standards and Technology, nor is it intended to imply that the entities, materials, or equipment are necessarily the best available for the purpose.

AMMT Scan Strategies

The AMMT is a facility at NIST which enables flexible and well-characterized monitoring and control of the laser powder bed fusion (LPBF) process [9,10]. AMMT control adapts an open platform design, using stereolithography (STL) files, G-code, and xy2-100 industrial standards for parts definition, path description, and galvanometer control, respectively. Figure 1 shows a generic software architecture for the AM system. The highlighted parts are modules implemented for AMMT. The step 3 'G-code Generator' converts a two-dimensional shape into scan paths described by G-code [11]. A standard G-code line, traditionally used for numerically controlled machines, describes a 'move' with destination point and speed. The LPBF-specific G-code version for NIST AMMT also includes laser power information. Step 4 'G-code Interpreter' translates this G-code into xy2-100 commands per the predefined interpretation mode. Xy2-100 commands [9,10] are digital positions updated every 10 μs to control a laser unit and galvanometer scanner. Therefore, the laser scan strategies are implemented by both 'G-code Generator' and 'G-code Interpreter'.

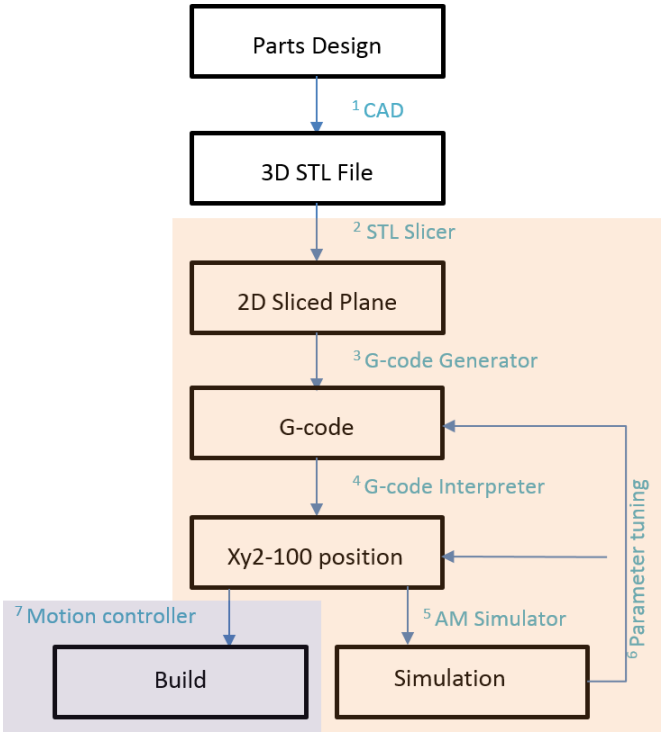

Figure 1: AMMT control design

G-code Generator

To build a layer, a two-dimensional shape must be filled up with scan vectors (hatching) which are spaced densely enough to melt the powder into a joint solidified region. The hatching pattern can be linear or concentric as shown in Figure 2a. The hatching lines can be scanned in an interleaved manner, or sequentially with alternative power as shown Figure 2b. A larger scan area can also be divided into smaller sub-regions (islands) and scanned in a certain sequence (Figure 2c). The combinations of above form the hatching strategy. G-code Generator fills a two-dimensional shape with scan vectors per the predefined hatching strategy, and generates G-code representing the scan vectors.

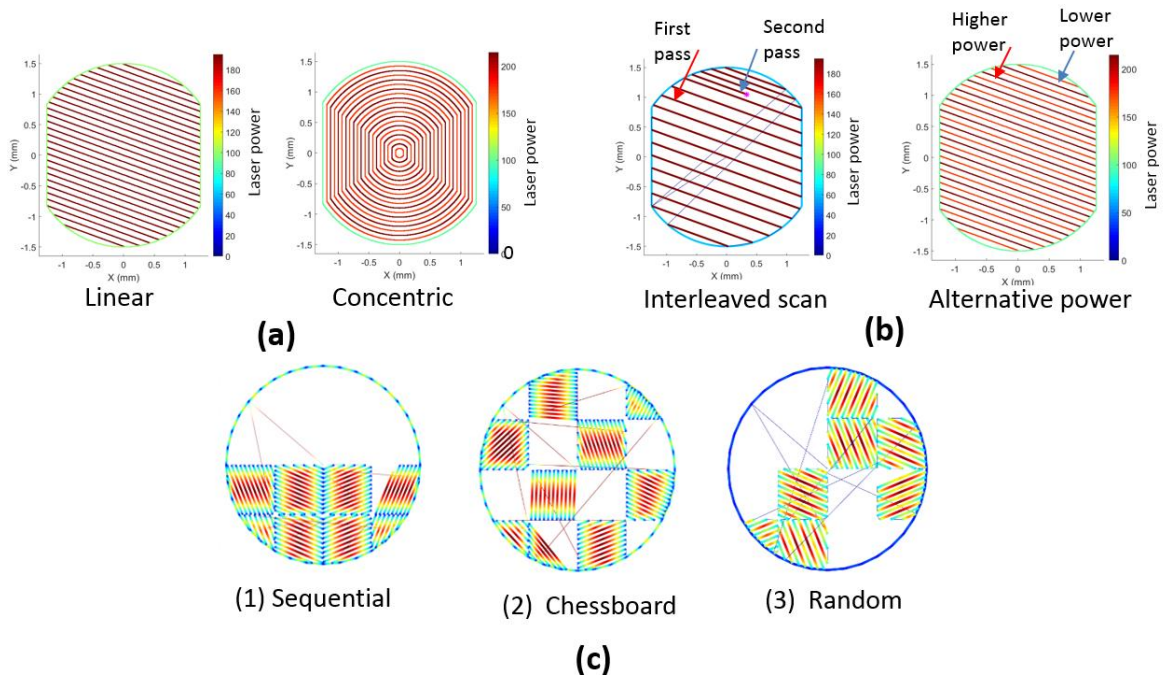

Figure 2: NIST AMMT hatching strategies: (a) Linear and concentric hatching patterns. (b) Interleaved scan and alternative power scan. (c) Islands with different scan sequence.

G-code Interpreter

The motion and power control of the laser spot within a move, as well as the transition between two sequential moves, is implemented in G-code Interpreter. Earlier work by the authors [9] proposed three laser path modes and three laser power modes. A summary is given below.

a) Laser path mode
   1. Exact stop mode – motion stops exactly at the end of each move with maximum allowable deceleration. If there is a subsequent move, motion will start immediately again with maximum allowable acceleration until it reaches the programmed speed, or until it needs to decelerate again.
   2. Constant build speed mode – motion is kept at constant speed for the whole move, if the laser power is on for that move (i.e., a build move). In order to achieve that, extra moves may be added before or after the original move to speed up or slow down the motion, but laser power is kept off for the added moves.
   3. Continuous mode - two sequential moves of different velocities are connected by an arc to allow a smooth transition of velocity. Deviation from the designed path within the maximum tolerance is allowed.

b) Laser power mode
   1. Constant power mode – power is kept constant at the programmed level during each build move, regardless of scan speed. If a subsequent move has a different power level, control sets the power to the new level.
   2. Constant density mode - power/speed ratio (power density) is kept at a predefined constant during each move. This constant is not necessarily the same for all moves.
   3. Thermal adjusted mode - power level is adjusted according to the predefined thermal properties of the building process.

Experiment design

Different scan strategies can be programmed on AMMT by the combination of hatching strategies, laser path modes, and laser power modes. Seven experiments were designed. Figure 3 shows the actual laser scan tracks from each experiment. All experiments were conducted on a ground stainless-steel plate (100 mm x 100 mm x 6.4 mm) without powder. The scan speed is 500 mm/s, power is 200-watt constant, and hatch spacing is 200 µm. Wider spacing is used so individual tracks can be observed. Table 1 lists scan area (length x width) and scan strategy for each experiment. Experiment 1, 4, and 5 used constant build speed mode, also known as 'sky-writing' on some commercial LPBF systems, and are therefore marked as conventional and used as a base line for comparison. Others are marked as 'AMMT' in Table 1 as authors are not aware of any similar scan strategies on commercial systems, although this does not mean that similar concepts have not been explored before [12,13].

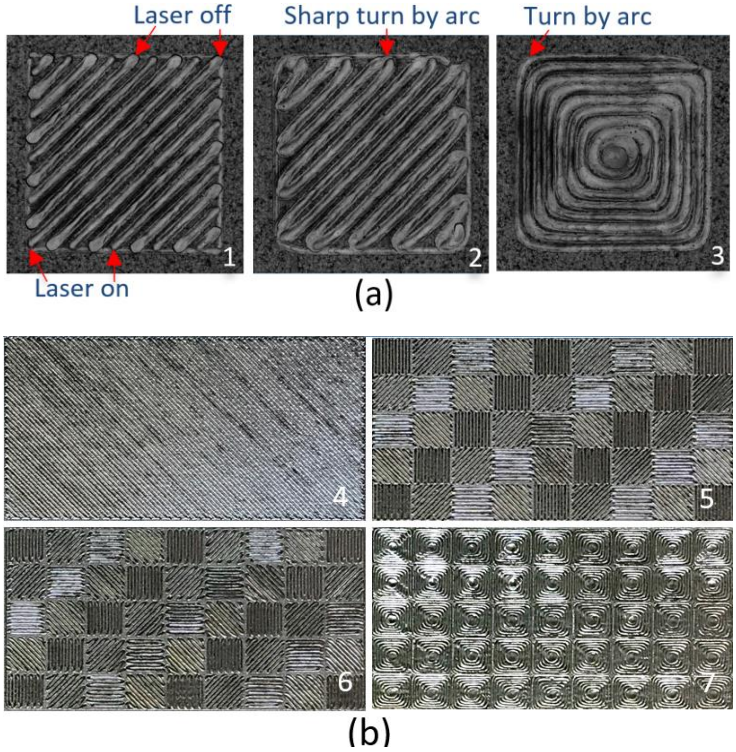

Figure 3. Scans on stainless steel plate with 500 mm/s speed and 200-watt constant laser power. (a) Single square scan experiments 1-3. (b) Island scan experiments 4-7.

Table 1. Experiment parameters

Exp #	Length x Width (mm)	Scan Strategies	Remarks
1	2.5 x 2.5	*Constant build speed*	Conventional
2	2.5 x 2.5	*Continuous linear*	AMMT
3	2.5 x 2.5	*Continuous concentric*	AMMT
4	20 x 10	*Constant build speed*	Conventional
5	20 x 10	*Constant build speed - island*	Conventional
6	20 x 10	*Continuous linear - island*	AMMT
7	20 x 10	*Continuous concentric - island*	AMMT

Melt-pool Analysis

A key signature characteristic in LPBF AM processes is the melt-pool geometry. One can observe the melt-pool to study the influence of laser control on the process. In this study, in-situ high-speed coaxial imaging is used to measure the melt-pool area, and post-process confocal laser scanning microscopy is used to measure the melt-pool height.

Melt-pool width measurement

To measure melt-pool area, a high-speed camera was setup coaxially with the laser beam using a dichroic mirror, imaging lens, and filter. Emitted light from the melt-pool, which is filtered at 850 nm (40 nm bandwidth), is imaged on the camera sensor with nominal 1:1 magnification and 20 μm pixel size. The camera is set to 50 000 frames/s, 10 μs exposure time, 128 pixel x 128 pixel window, and 8-bit dynamic range (grayscale). The gray levels are used to relate to melt-pool dimensions [14]. Contours, representing isotherm lines, can be drawn on the raw melt-pool image to represent equal intensity (Figure 4). A contour with intensity of 50 digital levels was found to equate to the physical melt pool width based on the ex-situ measured scan track width via microscope inspection. This digital level contour is then used to infer the melt pool boundary from the high-speed images and to calculate melt pool dimensions and area.

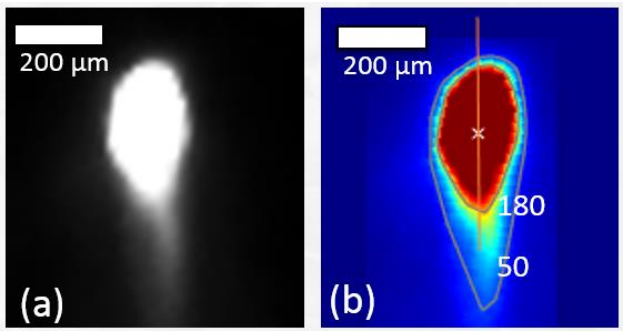

Figure 4. Melt-pool image analysis. (a) raw grayscale image. (b) processed image. Gray contour lines show different intensity levels (DL); red line shows melt-pool orientation.

Melt-pool height measurement

Confocal laser scanning microscopy enables the reconstruction of three-dimensional surfaces from a set of images obtained at different focal depths. A topography of the scan track such as Figure 5a can hence be created, with depth (height) represented by color. It is a very useful tool to visualize the effects of scan strategy on surface profile. From the topography, scan tracks are always bounded by valleys (Figure 5b), likely caused by surface tension of the molten metal. Once the two boundary valleys are identified, the melt-pool height can be defined as the peak between these two valleys (Figure 5c). Ideally the melt-pool width can also be determined by distance between the two valleys, but surface roughness or unsteady melt-pool behavior can sometimes create a local minimum (valley), too. Nevertheless, the local maximum is generally unique, making it a reliable approach for melt-pool height detection.

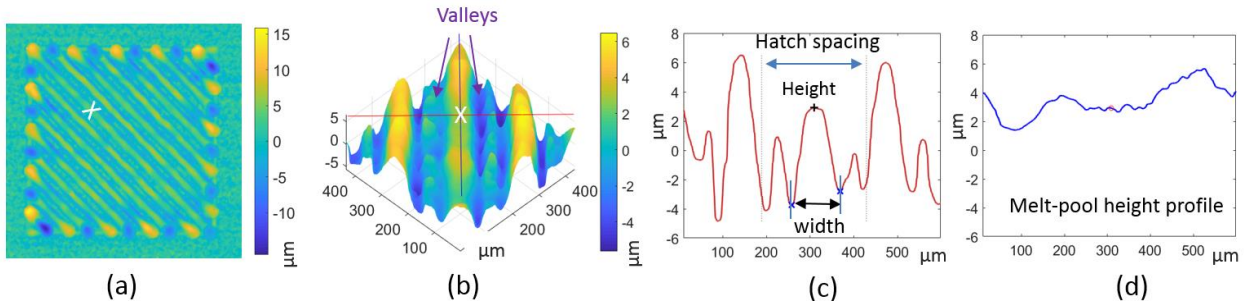

Figure 5 Melt-pool width and height detection from confocal microscopy. (a) Topography of the melt track from Exp. 1. (b) 400 μm x 400 μm three-dimensional plot centered at position marked by white x. (3) Cross section profile along the red line on three-dimensional plot. (d) Profile along the blue line.

Experiment results and discussion

Experiments 1-7 were conducted using AMMT on a bare metal (stainless steel) plate; no powder was added. The microscopic images of the scanned regions were shown in Figure 3. The processes were in-situ imaged by the high-speed coaxial camera at 50 000 frame/s with 10 μs exposure time. The images were processed to obtain melt-pool area, with the results plotted in Figure 6. The scanned regions were then examined by confocal microscope. The surface profiles are plotted in Figure 7 and Figure 8. The surface profile of an un-scanned region on the metal plate is also shown in Figure 7 as a reference.

Figure 6 shows the melt-pool area from the high-speed coaxial image analysis. Dark lines plot melt-pool areas for each individual frame, and red lines are the means for each experiment with one standard deviation. Table 2 lists mean, standard deviation, and build time specified for each experiment.

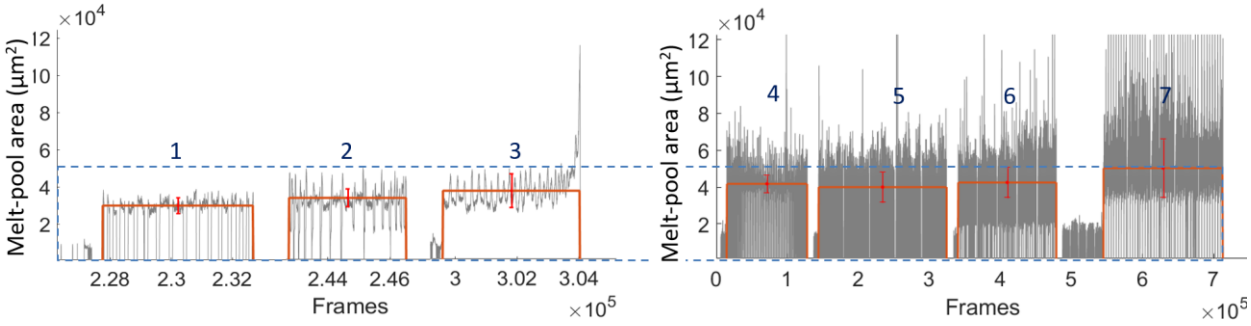

Figure 6 Melt-pool area measurement from coaxial high-speed image analysis. (a) Single square scan experiments (Exp. 1-3). (b) Island scan experiments (Exp. 4-7).

Table 2. Average melt-pool area, standard deviation, and build time for Exp. 1-7.

Exp. #	1	2	3	4	5	6	7
Mean melt-pool area (μm^2)	*29900*	*33300*	*39700*	*41700*	*40000*	*42500*	*50300*
Standard deviation (μm^2)	*4400*	*4700*	*8900*	*4700*	*8300*	*8100*	*15900*
Build time (s)	*0.098*	*0.076*	*0.088*	*2.258*	*3.600*	*2.758*	*3.356*

Based on the in-situ melt pool imaging, and ex-situ topography results, the following observations are made:

1. For single square scans (Exp. 1-3), continuous linear mode is the most time efficient, while continuous concentric mode has the largest mean melt-pool area. The increasing melt-pool area for Exp. 3 (Figure 6) should be due to the residual heat building up as concentric circles are getting smaller.
2. For multi-square island scans (Exp. 5-7), the trend is consistent with single square scans. The time for continuous linear mode (Exp. 6) improved by 23% over constant build speed mode (Exp. 5), and average melt-pool size for continuous concentric mode (Exp. 7) improved by 25% over constant build speed mode (Exp. 5).
3. Island scans (Exp. 4-7) yield a larger melt-pool area than their single square counterparts (Exp. 1-3). Longer scan time and more localized scan path helped build up the residual heat.
4. Comparing Exp. 4 with 5, island scan strategy does not seem to have any advantage for constant build speed mode, in terms of both building time and melt-pool size. The laser was turned on and off very frequently for Exp. 5 because of the shorter scan distance. That might have balanced out the localized heat effect of the island scan.
5. The standard deviations of the melt-pool areas are the smallest for Exp. 1 and 4. The power density is more consistent in constant build speed mode.

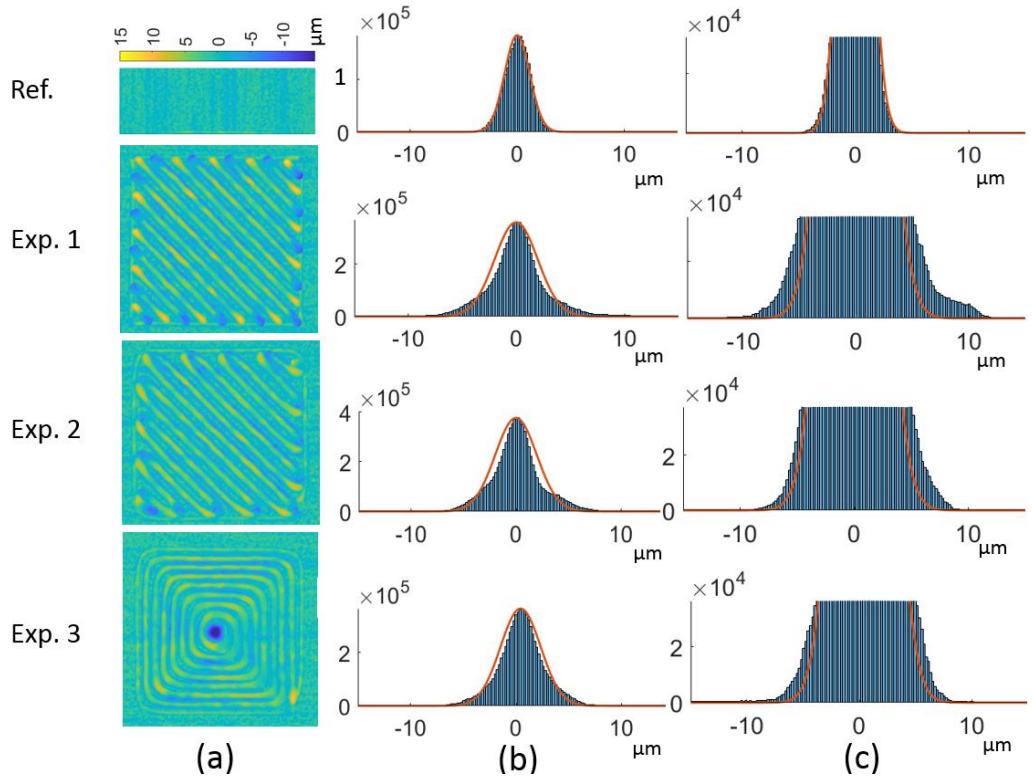

Figure 7. Surface profiles for Exp. 1-3. (a) Topographies. (b) Histogram of height data with normal distribution curve fitted. X-axis is the height in μm, Y-axis is number of points. (c) Enlarged view of (b).

Figure 7a shows the topographies for Exp. 1-3, and a reference region (an un-scanned area on the same metal plate). Figure 7b is the distribution of the height for each point on the topography. Figure 7c is an enlarged view of Figure 7b, and shows how the height data spread out around boundaries. The height profile for the reference fits very well into a normal distribution curve, which represents the surface

roughness of the original metal plate. All experiments resulted in a 'rougher' surface as the height data spread wider (Figure 7b and Figure 7c), especially for Exp. 1 which goes beyond +/- 10 µm range. A rougher surface may end up a poorer part quality in a three-dimensional build as it prevents even distribution of powder, or it may even jam the recoater blade. To further visualize how different scan strategies affect the surface profile, the top left corners of each experiment were enlarged and compared in Figure 8.

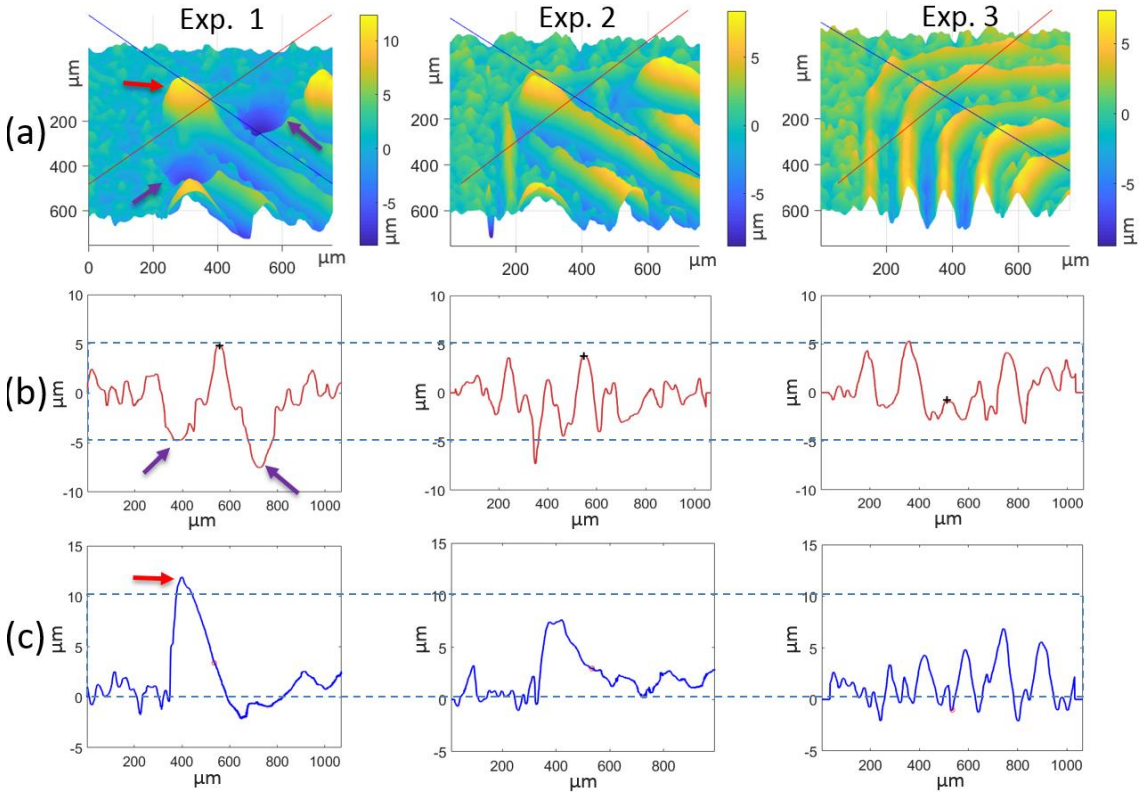

Figure 8. Surface profiles for Exp. 1-3. (a) Topographies. (b) Height profile along the red line. (c) height profile along the blue line.

For constant build speed mode (Exp. 1), the laser power was turned on at the beginning and turned off at the end for each scan line. That created bumps at the beginnings and holes at the ends, as indicated by the red and purple arrows in Figure 8a. Continuous linear mode (Exp. 2) reduces the laser on and off frequency, but the sharp turn between adjacent hatch lines creates complicated local thermodynamics. That still resulted in 'valleys' around turns, but at a smaller scale compared to Exp. 1. The continuous concentric mode (Exp. 3) has no sharp turns (except at the center), resulting in the most even surface, as shown in Figure 8b and Figure 8c.

Summary and Future work

There is an open field of research into laser scan strategy with the potential to reduce defects, control residual stress or microstructure, or improve the speed and efficiency of material consolidation. The NIST AMMT provides control and monitoring capabilities for such research. This paper demonstrated two advanced scan strategies implemented on AMMT – continuous linear and continuous concentric. The results show clear advantages over traditional (constant build speed) scan strategy for both efficiency and

quality. The build time for the continuous linear strategy is 23% faster than the traditional strategy, and the continuous concentric strategy effectively reduced bumps and holes compared to the traditional strategy.

Constant laser power was used for all experiments in this work, although AMMT has the capability for adjusting laser power at 100 kHz. A proper tuning of laser power should be able to further improve the surface quality. It is also shown here that a continuous island scan produced a larger melt-pool, and the island scan is believed to be able to reduce residual stress as well. A study of multilayer powder builds based on varying power continuous concentric island scans should be very interesting.

References

[1] Mani M, Lane B, Donmez M A, Feng S, Moylan S and Fesperman R 2015 *Measurement science needs for real-time control of additive manufacturing powder bed fusion processes* (Gaithersburg, MD: National Institute of Standards and Technology)

[2] King W E, Barth H D, Castillo V M, Gallegos G F, Gibbs J W, Hahn D E, Kamath C and Rubenchik A M 2014 Observation of keyhole-mode laser melting in laser powder-bed fusion additive manufacturing *J. Mater. Process. Technol.* **214** 2915–25

[3] Thijs L, Verhaeghe F, Craeghs T, Humbeeck J V and Kruth J-P 2010 A study of the microstructural evolution during selective laser melting of Ti–6Al–4V *Acta Mater.* **58** 3303–12

[4] Yadroitsev I, Thivillon L, Bertrand P and Smurov I 2007 Strategy of manufacturing components with designed internal structure by selective laser melting of metallic powder *Appl. Surf. Sci.* **254** 980–3

[5] Khairallah S A, Anderson A T, Rubenchik A and King W E 2016 Laser powder-bed fusion additive manufacturing: Physics of complex melt flow and formation mechanisms of pores, spatter, and denudation zones *Acta Mater.* **108** 36–45

[6] Cheng B, Shrestha S and Chou K 2016 Stress and deformation evaluations of scanning strategy effect in selective laser melting *Addit. Manuf.* **12** 240–51

[7] Gockel J and Beuth J L 2013 Understanding Ti-6Al-4V microstructure control in additive manufacturing via process maps *Solid Freeform Fabrication Proceedings* Solid Freeform Fabrication Proceedings (Austin, TX) pp 666–74

[8] Mercelis P and Kruth J-P 2006 Residual stresses in selective laser sintering and selective laser melting *Rapid Prototyp. J.* **12** 254–65

[9] Yeung H, Neira J, Lane B, Fox J and Lopez F Laser Path Planning and Power Control Strategies for Powder Bed Fusion Systems *Solid Free. Fabr. 2016 Proc. 27th Annu. Int. Solid Free. Fabr. Symp.*

[10] Lane et al. Design, Developments, and Results from the NIST Additive Manufacturing Metrology Testbed (AMMT) *Solid Free. Fabr. 2016 Proc. 26th Annu. Int. Solid Free. Fabr. Symp.*

[11] Electronic Industries Association Interchangeable Variable Block Data Format for Positioning, Contouring, and Contouring/Positioning Numerically Controlled Machines *EIA Stand. EIA-274-Febr. 1979*

[12] Carter L N, Martin C, Withers P J and Attallah M M 2014 The influence of the laser scan strategy on grain structure and cracking behaviour in SLM powder-bed fabricated nickel superalloy *J. Alloys Compd.* **615** 338–47

[13] Kruth J P, Froyen L, Van Vaerenbergh J, Mercelis P, Rombouts M and Lauwers B 2004 Selective laser melting of iron-based powder *J. Mater. Process. Technol.* **149** 616–22

[14] Rombouts M, Kruth J-P, Froyen L and Mercelis P 2006 Fundamentals of selective laser melting of alloyed steel powders *CIRP Ann.-Manuf. Technol.* **55** 187–92